Scattering efficiency of aggregated clusters of spheres: dependence on configuration and composition

Jean-Claude Auger

Centro de Investigación en Polímeros, Grupo COMEX, Boulevar M.A. Camacho No 138, Lomas de Chapultepec, 11560 Mexico D.F., México

Brian Stout

Institut Fresnel, Centre de St. Jérôme UMR 6133, 13397 Marseille Cedex 20, France

Vincent Martinez

Centro de Investigación en Polímeros, Grupo COMEX, Boulevar M.A. Camacho No 138, Lomas de Chapultepec, 11560 Mexico D.F., México

Received January 27, 2005; revised manuscript received May 31, 2005; accepted June 1, 2005

We study the orientation average scattering cross section of various isolated aggregates of identical spherical particles as functions of their size, optical properties, and spatial configurations. Two kinds of aggregates are studied: latex particles in water and rutile titanium dioxide pigments in a polymeric resin, with size parameters varying from 0.6 to 2.3. Calculations are performed by using a recursive centered T-matrix algorithm solution of the multiple scattering equation that we previously developed [J. Quant. Spectrosc. Radiat. Transfer **79–80**, 533 (2003)]. We show that for a specific size of the constituent spheres, their respective couplings apparently vanish, regardless of the aggregate configuration, and that the scattering cross section of the entire cluster behaves as if its constituents were isolated. We found that the particular radius for which this phenomenon occurs is a function of the relative refractive index of the system. We also study the correlations between the strength of the coupling among the constituent spheres, and the pseudofractal dimension of the aggregate as it varies from 1 to 30.

OCIS codes: 290.4020, 290.4210, 290.5850.

1. INTRODUCTION

The study of the optical properties of granular materials is a subject of broad interest on account of the various applications that can be encountered in academic research and industry. Numerous studies have already been performed concerning, for example, remote atmospheric sensing[1] or the characterization of interstellar dust and its effect on the propagation of stellar radiation in astrophysics.[2] Also, various theoretical approaches have been proposed to calculate light scattering properties by clusters composed of spheres having sizes comparable with the wavelength of the incident field.[3,4] Numerous studies have been conducted in the quasi-static approximation, for example to reproduce experimental Raman scattering data obtained for silica aerogels[5] or to study resonant extinction in colloidal systems containing either nonabsorbing or strongly absorbing spherical particles.[6] From the industrial point of view, such as in the coating industry, manufacturers study the influence of aggregation and flocculation phenomena of rutile titanium dioxide pigment on opacity and gloss of dried paint films.[7]

Optical properties of inhomogeneous media can be studied at two levels. On the microscopic scale, one is typically concerned with the scattering and/or absorption processes that occur between the incident radiation and the heterogeneities of the dispersed phase. In such studies, the nature, size, shape, orientation, volume fraction, and spatial dispersion of the scatterers are the primary parameters affecting the physical response. The principal theoretical challenge is then to relate such variables to the amplitude scattering matrix elements and total cross sections of the volume element of the medium under study.

Rayleigh[8] and Mie[9] introduced the first formalisms to describe the interaction of a monochromatic plane wave with isolated dielectric or metallic spherical particles embedded in a nonabsorbing media. Subsequently, numerous other formalisms were developed in order to calculate the light scattering and absorption properties of nonspherical or aggregated particles. Among the most prevalent are the discrete dipole approximation,[10] the T-matrix formalism,[11,12] the finite-element method,[13,14] and the finite-difference time-domain method.[15–17]

On the macroscopic scale, optical properties such as the total reflection and transmission coefficients, in addition to having a dependence on the local parameters cited above, also have a strong dependence on the thickness of the medium, the roughness of the interfaces, and the type

of illumination. They are generally evaluated from the radiative transfer equation formalism[18] or the analytical theory of the multiple scattering equation.[19]

If limited computing capabilities at first prevented or limited exhaustive multiple scattering studies, nowadays, they can be performed much more rapidly. Typical studies consist in analyzing the correctness and consistency of theoretical predictions through comparisons with experimental measurements[20] or in the characterization of the dispersion medium.[21] One can also perform systematic studies relating the change in optical properties of a well-defined system as a function of the variation of one or several key parameters, allowing a better understanding of the fundamental processes under study.[22] In this work, we focus on the latter approach and study the relation between the orientation average scattering cross section of clusters composed of aggregated spherical particles and their configurations. Such studies are usually applied within the quasi-static approximation by using the discrete dipole approximation[23,24] or within an approximation of the analytical theory of multiple scattering.[25] Here, we propose a numerical study in the Mie scattering regime by using a recursive centered T-matrix algorithm (RCTMA)[26] that is an exact solution of the vector multiple scattering equation.[27]

As our primary concern is the optical properties of architectural white paint films, our study is applied to systems composed of rutile titanium dioxide pigments in a polymer resin and latex particles in water. Nevertheless, the methodology and principal results that we encountered could be useful in the different fields of research mentioned earlier. The reason for studying such systems is that water-based architectural paints are composed of a combination of Latex emulsions and rutile titanium dioxide suspensions. Both colloidal systems are thermodynamically unstable, and eventually, dispersion forces will lead to flocculation and sedimentation. Stability can be promoted with surface-active agents, also called surfactants, that adsorb on the particle surface and prevent aggregation by means of electrostatic and/or steric repulsions. Nevertheless, cluster formation cannot be totally avoided, and its presence affects the performance of the paint. Rutile titanium dioxide aggregates decrease the opacity of white paint, whereas flocculation of latex particles can lead to a premature coalescence of the polymer chains. Also, emulsion stability is often monitored by measuring particle size distribution with dynamic light scattering. It is therefore important and of interest to study the optical properties of such systems as functions of cluster characteristics such as size, shape, and configuration.

The paper is constructed as follows: In Section 2, we briefly introduce the multiple scattering theory that has been used throughout the numerical study. Section 3 is devoted to the description of the cluster generation process, the presentation of the statistical analysis that we performed, and the associated data treatment that we applied. Section 4 is dedicated to the presentation of the main results and to the discussion of the principal effects encountered. To clarify the discussion, the concept of transition radius and the possible extrapolation of our results to much larger clusters are studied in two different paragraphs. Finally, in Section 5, we conclude with our final observations and comments.

2. THEORY

To calculate the orientation average scattering cross section of an ensemble of aggregated dielectric or metallic spheres immersed in an infinite nonabsorbing medium, we adopted a multiple T-matrix formalism[26] of the multiple scattering equation.[27,28] In this approach, the incident, internal, and scattered electromagnetic fields are expanded in terms of vector spherical wave functions and one associates with each particle in the system both single T matrices $\bar{T}^{i(1)}$ and multiple scattering T matrices $\bar{T}^{i(N)}$ (i being the particle label).

The $\bar{T}^{i(1)}$ characterize the intrinsic optical properties of the isolated scatterers and can be calculated from the extended boundary condition technique introduced by Waterman.[10] The multiple scattering T matrices $\bar{T}^{i(N)}$ are obtained from a complete solution of the multiple scattering equations and describe the optical response of a scatterer while taking into account the presence of all the other particles. In our formalism, the $\bar{T}^{i(N)}$ satisfy the equation

$$\bar{T}^{i(N)} = \bar{T}^{i(1)}\left[\bar{I} + \sum_{\substack{j=1 \\ j\neq i}}^{N} \bar{H}^{(i,j)}\bar{T}^{j(N)}\bar{J}^{(j,i)}\right], \qquad i = 1, \ldots, N, \quad (1)$$

where $\bar{J}^{(i,j)}$ and $\bar{H}^{(i,j)}$ are the matrices that translate the incident and the scattered fields, respectively, from the ith to the jth reference frames.[29] We solved Eq. (1) with a RCTMA that we have introduced in previous works.[26,27] In this formalism, the $\bar{T}^{i(N)}$ matrices can be expressed in terms of centered T matrices, denoted $\bar{\tau}_N^{(i,j)}$ such that

$$\bar{T}^{i(N)} = \sum_{j=1}^{j=N} \bar{\tau}_N^{(i,j)}\bar{J}^{(j,i)}. \quad (2)$$

The fundamental relations of the RCTMA are given in Appendix A. A great advantage of multiple T-matrix formalism is that one can easily perform an analytical evaluation of the orientation average cross section of the system under study.[30] In the present work, we study nonabsorbing particles for which the scattering cross section is equal to the more simply formulated extinction cross section that can be expressed[31] as

$$\langle C_{ext}\rangle = \frac{2\pi}{k_0^2}\mathrm{Tr}\sum_{i=1}^{N}\sum_{j=1}^{N}\bar{\tau}_N^{(i,j)}\bar{J}^{(j,i)}, \quad (3)$$

where k_0 is the wave vector of the incident radiation and Tr stands for trace. Once the position, size, and complex index of refraction of each sphere is given, one can use Eqs. (A1)–(A4) in Appendix A to calculate the centered T matrix associated with each scatterer. Finally, with Eq. (3) the orientation average extinction cross section of the system can be evaluated.

3. CLUSTER CONFIGURATION AND DATA TREATMENT

A. Cluster Configuration

In a previous work,[32] we calculated the orientation average scattering cross section (OASCS) of linear and compact arrangements of aggregated spheres of rutile titanium dioxide with radii ranging from 0.04 to 0.132 μm. The compact configurations in these studies were constructed from simple crystalline lattice models. Conclusions of this work were that the OASCS showed three distinctive behaviors as functions of the particle radii: Near $r_s \cong 0.08$ μm, the OASCS of the aggregate was very close to the sum of the scattering cross sections of the isolated spheres, and for larger and smaller radii, the OASCS was smaller and larger than the independent scattering sum, respectively.

In this work, we study the influence of the cluster arrangements on the OASCS for more realistic configurations than those studied previously. For this purpose, in addition to linear arrangements of spheres, we have studied clusters formed from two different aggregation processes.[33] The first model is the diffusion-limited cluster–cluster aggregation (DLCCA). It assumes that the colloids stick permanently as soon as they touch, and thus the mechanism is limited by the time taken for the particles to diffuse through the suspension and meet. Such a mechanism leads to clusters with fractal dimension of $f_d \cong 1.8$. The second model, known as the reaction-limited particle–cluster aggregation (RLPCA), assumes that the particles do not necessarily stick at first contact and that they can rearrange themselves. Thus, the aggregation process is limited by the time taken for a sticking encounter to occur. Such an assumption leads to more compact clusters than those in the previous model, with fractal dimension close to $f_d \cong 3.0$.

B. Numerical Calculations and Data Treatment

The different aggregates were generated thanks to a FORTRAN source code provided by R. Botet. Based on the variations of the OASCS as a function of particle size observed in our previous study, the sizes of the constituent spheres studied were chosen as $r_s = 0.04$, 0.08, and 0.132 μm for each fractal dimension (linear, DLCCA, and RLPCA). The wavelength of the incident radiation was taken as 0.546 μm corresponding to the center of the visible range. The complex indices of refraction were taken to be 1.5 for the latex particles and polymer resin and 1.33 for water. Rutile titanium dioxide is birefringent and thus possesses two distinctive indices of refraction. For the purpose of this study, we choose a commonly used approximation[34] that consists of a weighted average of both indices, which yields 2.8 for the chosen wavelength. The indices of the particles and of the surrounding medium are denoted n_s and n_m, respectively.

Once the aggregates were generated (Figs. 1 and 2), the following methodology was applied: We calculated the OASCS associated with 1000 different configurations of the DLCCA and RLPCA families of clusters composed of 6, 9, 12, 15, 18, and 21 spheres with particle radii of 0.04, 0.08, and 0.132 μm for both systems. Figure 3 represents the OASCS, also denoted $\langle C_{ext} \rangle$, determined in the differ-

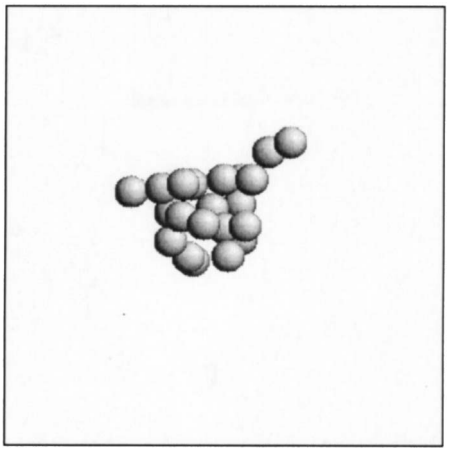

Fig. 1. Aggregate composed of 21 spheres generated from the RLPCA process.

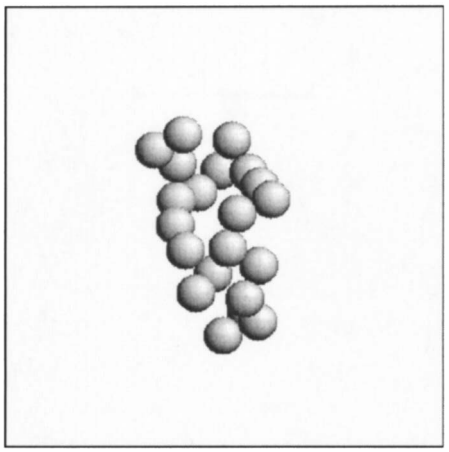

Fig. 2. Aggregate composed of 21 spheres generated from the DLCCA process.

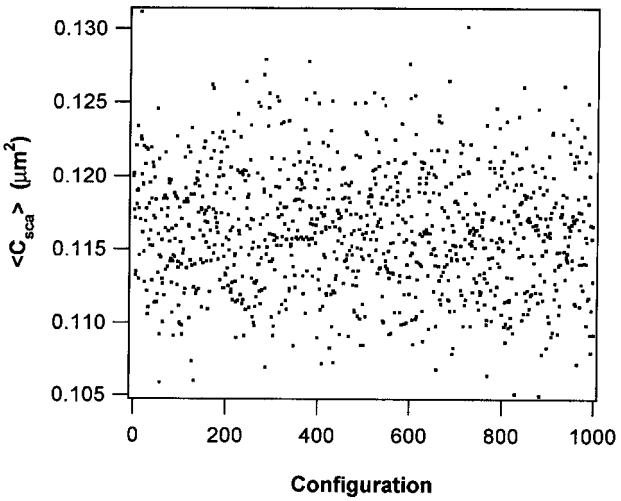

Fig. 3. OASCS $\langle C_{sca} \rangle$ as a function of 1000 different configurations. The aggregates are composed of 12 spheres of radius $r_s = 0.132$ μm generated from the RLPCA process with index of refraction $n_s = 1.5$ embedded in water with index of refraction $n_m = 1.33$. The wavelength of the incident radiation is 0.546 μm.

ent configuration trials for a 12-sphere cluster of latex particles in water, generated from the RLPCA process. Histograms (Fig. 4) of the occupation number were then constructed and fitted with a Gaussian probability function by adjusting the average cross section $\langle C_{ext}\rangle_c$ and the standard deviation σ_c. The $\langle C_{ext}\rangle_c$ represents the configuration average of the OASCS, while σ_c describes the deviation from this average value of the statistical ensemble. To check the reliability of the sample number, we performed the same adjustments on an ensemble of 3000 configurations. Relative errors inferior to 1% were found on $\langle C_{ext}\rangle_c$ and σ_c, allowing us to conclude that 1000 configurations represent a sufficiently accurate sampling of the possible configurations for each family.

4. RESULTS AND DISCUSSION

Figures 5(a), 5(b), and 5(c) represent the Gaussian adjustments related to the occupation probabilities of the 6-, 9-, 12-, 15-, 18-, and 21-sphere clusters of rutile titanium dioxide immersed in the polymer resin, as functions of the OASCS. The radii of the constituent spheres are respectively $r_s=0.04$, 0.08, and 0.132 μm, whereas the solid and dashed curves are associated with clusters generated from the DLCCA and RLPCA aggregation processes, respectively. Also, because all adjustments are calculated from the same number of different configurations, the corresponding areas under each Gaussian fit are identical.

The case of linear clusters is particular and much simpler to treat, since only one configuration is possible. The latter leads to $\langle C_{ext}\rangle_c=\langle C_{ext}\rangle$ and $\sigma_c=0$, and consequently no Gaussian adjustment is necessary. Also, in order to study the electromagnetic coupling between the constituent spheres, we have represented in Figs. 6(a), 6(b), and 6(c) the variation of $\langle C_{ext}\rangle_c$ as a function of the number of particles for the independent-spheres assumption, the RLPCA, DLCCA, and linear aggregates with a radius of 0.04, 0.08, and 0.132 μm, respectively. Let us recall that in the independent scattering assumption, the scattering cross section of the aggregate is calculated supposing that each constituent sphere scatters light as if it were isolated. In this case, one has $\langle C_{ext}\rangle=N_s C_{ext}^I$ and $\sigma_c=0$, where C_{ext}^I represents the scattering cross section of an isolated particle.

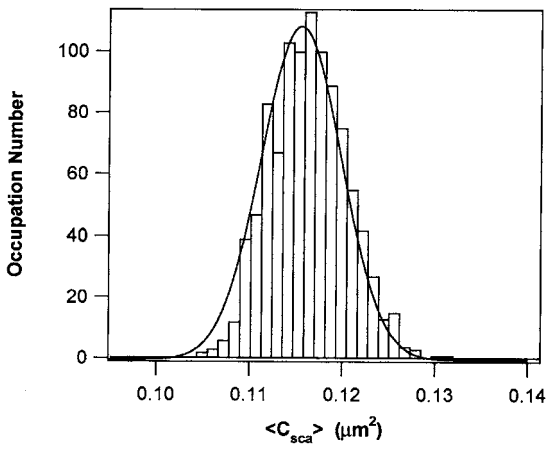

Fig. 4. Histogram constructed from the values of Fig. 3, where the occupation frequency is plotted as a function of $\langle C_{sca}\rangle$ and fitted with a Gaussian probability function.

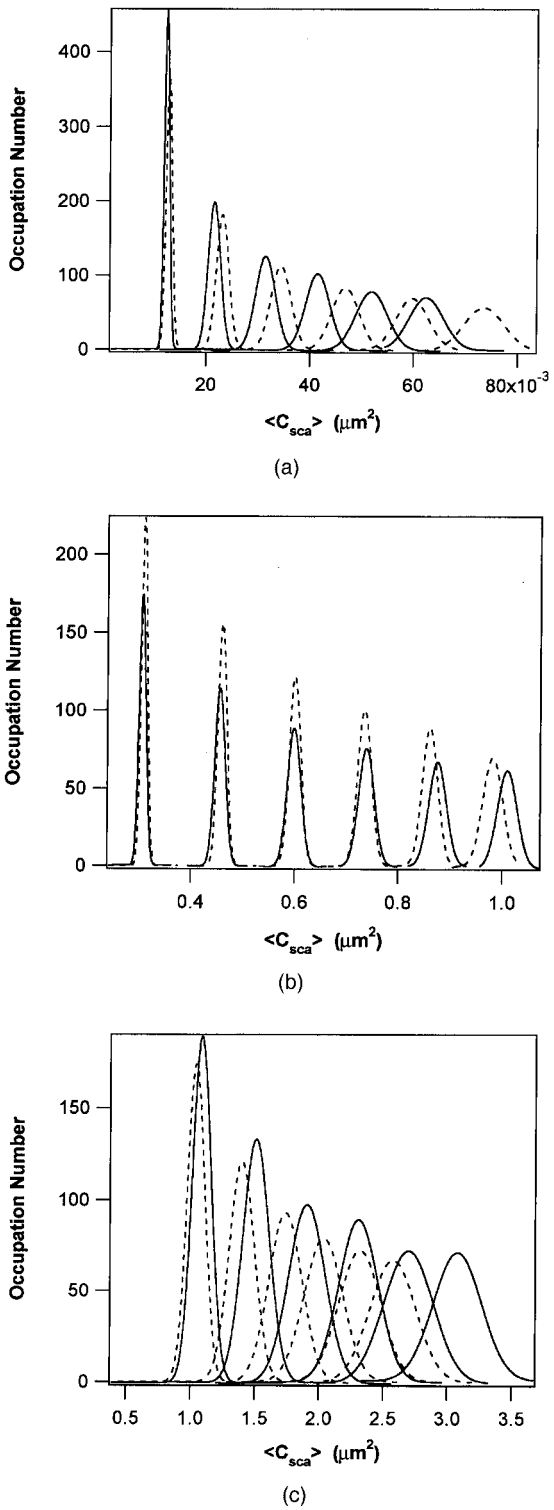

Fig. 5. Gaussian adjustments for the 6-, 9-, 12-, 15-, 18-, and 21-sphere clusters of rutile titanium dioxide ($n_s=2.8$) in a polymer resin ($n_m=1.5$) for 1000 different configurations. The solid and dashed curves indicate aggregates generated from the DLCCA and RLPCA, respectively. The radii of the spheres are equal to (a) 0.040 μm, (b) 0.080 μm, and (c) 0.132 μm.

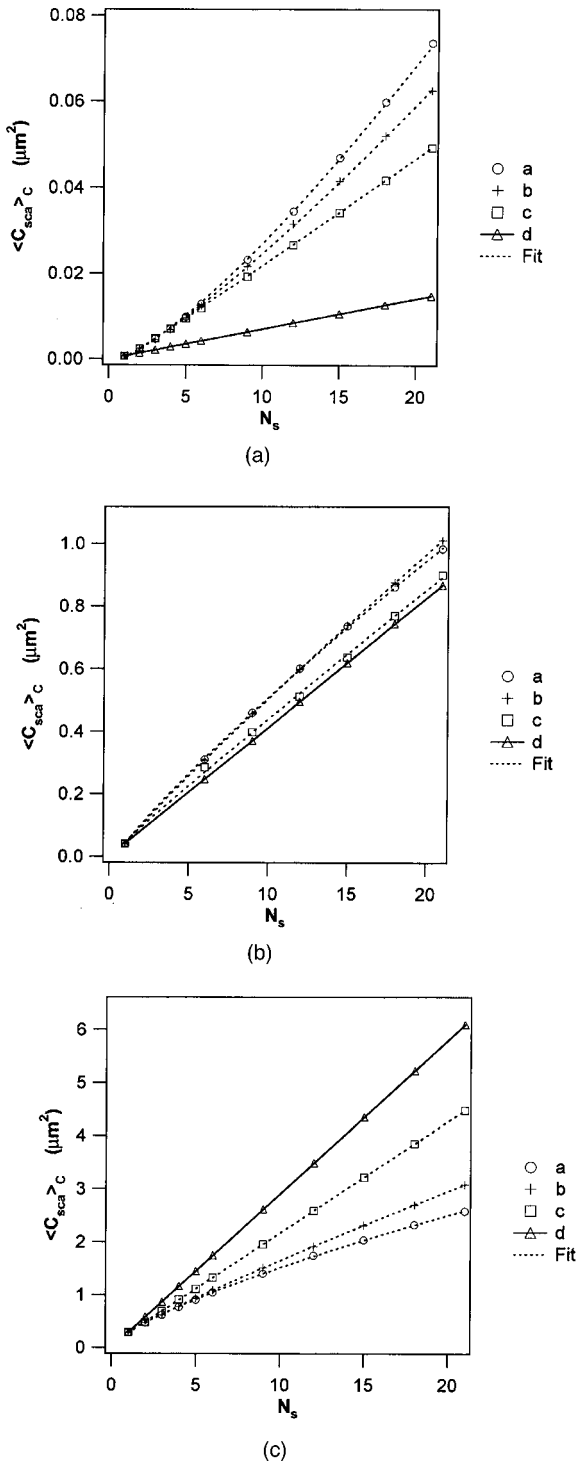

Fig. 6. (a) Variation of $\langle C_{ext}\rangle_c$ as a function of the number of particles for the (a) RLPCA, (b) DLCCA, and (c) linear chain with respective fractal dimensions of 3.0, 1.8, and 1.0, together with the value of $\langle C_{ext}\rangle_c$ in the case of isolated scatterers (d) for a cluster of rutile titanium dioxide particles in a polymer resin. The radius of the constituent spheres is $r_s=0.04$ μm. (b) Same as (a) but for $r_s=0.08$ μm. (c) Same as (a) but for $r_s=0.132$ μm.

A. Effects of the Number of Particles in the Cluster on the Orientation Average Scattering Cross Section

Inspection of Fig. 5 shows that the width σ_c and the averaged value $\langle C_{ext}\rangle_c$ of the probability distribution always increase as a function of the number of spheres N_s in the cluster. Indeed, since the incident radiation is a monochromatic plane wave of infinite spatial extent, the average amplitude of the scattering interaction process $\langle C_{ext}\rangle_c$ is directly related to the size of the scattering object. Also, for a small number of constituent spheres, the quantity of possible configurations is limited and both the DLCCA and RLPCA give rise to very similar aggregates.

Taking into account the discussion in previous paragraphs together with the fact that the incident radiation cannot discern the details of the cluster structure, at least insofar as their dimensions are smaller than the wavelength, the OASCS does not undergo large variations from one configuration to another, and σ_c remains small for small clusters. However, as the number of constituent spheres increases, the number of different configurations, as well as the overall dimension of the aggregates, also increases. For this reason, the optical response given by the OASCS is spread over a larger range of different values, inducing larger values of σ_c. As a consequence, there is an increase of the overlap zone between the Gaussian adjustments. This overlap is essentially negligible between the six- and nine-sphere clusters, whereas it is quite noticeable between the 18- and 21-sphere systems. In short, essentially none of the six-sphere configurations scatters with the same strength as that of the nine-sphere clusters, but numerous 18-sphere configurations have the same OASCS as that of aggregates composed of 21 particles.

B. Effects of the Cluster Pseudofractal Dimension on the Orientation Average Scattering Cross Section

We now focus on the comparison between the optical responses of clusters having the same number of constituent spheres but generated from different aggregation process. Inspection of Figs. 5(a) and 5(c) shows that values of σ_c are always larger for the RLPCA than for the DLCCA aggregates. Also, because of the condition of constant area under the Gaussian adjustments mentioned above, this implies that the occupation probabilities associated with the values of $\langle C_{ext}\rangle_c$ are always smaller for the former than for the latter. In other words, the denser the aggregate's configuration (higher pseudofractal dimension), the wider the optical response in term of OASCS. This phenomenon can be explained by assuming that the probability of the electromagnetic coupling is directly proportional to the average number of particles directly touching in the aggregates. Then, constituent spheres in clusters generated from the RLPCA process ($f_d=3$) undergo more coupling phenomena, and the resulting OASCS is spread over a larger range of possible values. Consequently, the pseudofractal dimension gives important information on the possible electromagnetic coupling between the constituent particles of the aggregates.

The aforementioned tendency clearly appears in an inspection of Figs. 6(a) and 6(c), where the differences between the values of $\langle C_{ext}\rangle_c$ for the linear, DLCCA, and RLPCA become more significant as the number of constituent spheres increases. For large numbers of particles, each type of aggregate has a different optical response, which indicates distinctions in the degree of electromagnetic couplings between constituent spheres.

The lower the pseudofractal dimension, the closer the response to the isolated case, whereas, the higher the fractal dimension, the larger the difference. In other words, superior and inferior limits of the variation of $\langle C_{ext}\rangle_c$ are given by the linear ($f_d=1.0$) and compact ($f_d=3.0$) cases. Between these limits, the optical response of different fractal dimensions follows the same tendency. Fractals having a variation of $\langle C_{ext}\rangle_c$ closest to the isolated scatterer response should have the lowest fractal dimension, whereas those with the larger discrepancies should have the higher fractal dimension.

C. Effects of the Size of the Constituent Spheres on the Orientation Average Scattering Cross Section

After having studied the influence of the clusters' pseudofractal dimension, we focus in this subsection on the effects of the size of the constituent spheres on the OASCS. From Figs. 5(a) and 5(c), it can be seen that at $r_s=0.04$ μm, RLPCA aggregates scatter on the average more than DLCCA clusters (higher values of $\langle C_{ext}\rangle_c$), whereas the opposite is true at $r_s=0.132$ μm. This behavior can also be illustrated by a careful analysis of the size of the normalized overlapping areas between the different Gaussian adjustments (Table 1), where the normalization is realized on the sum of both areas. It is seen that normalized overlapping areas between the $N_s=N$ and $N_s=N+3$ clusters, where $N=12$, 15, 18, and 21, is always larger for DLPCA than for RLPCA clusters at $r_s=0.040$ μm, whereas the opposite holds at $r_s=0.132$ μm. The strength and type of coupling between the constituent particles depends then not only on the configuration of the aggregate (and consequently on its fractal dimension), as shown previously, but also on the size of the constituent spheres.

One important feature also appearing from inspection of Figs. 6(a) and 6(c) is that for $r_s=0.132$ μm, all cluster families have $\langle C_{ext}\rangle_c$ values inferior to those of the isolated case whereas for $r_s=0.04$ μm they are all superior. Such behavior can be understood from Mie and Rayleigh scattering characteristics. In the $r_s=0.132$ μm case, the scattering intensity is associated with the total surface area of the cluster, which decreases when one particle is added to the system. For this reason, the effect is amplified as the pseudofractal dimension increases. In the $r_s=0.04$ μm case, particle dimensions are much smaller than the wavelength of the incident field, and the scattering intensity is proportional to scatterer size raised to the fourth power. Adding particles to the system will increase the scattering intensity compared with that in the isolated hypothesis. Finally, since the $r_s=0.04$ and $r_s=0.132$ μm cases respectively yield values of $\langle C_{ext}\rangle_c$ inferior and superior to those of the isolated system, one could assume that there exists one radius of the constituent spheres at which the OASCS of the coupled system is equal to the latter. This specific concept is discussed in detail in Subsection 4.D.

Table 1. Normalized Size of the Overlapping Areas for RLPCA and DLPCA Clusters

Particle Radius r_s (μm)	System	RLPCA	DLPCA
0.040	A[a]	0.003	0.008
	B[b]	0.012	0.026
	C[c]	0.025	0.050
0.132	A[a]	0.16	0.094
	B[b]	0.22	0.145
	C[c]	0.29	0.185

[a]Between the 12- and 15-sphere clusters.
[b]Between the 15- and 18-sphere clusters.
[c]Between the 18- and 21-sphere clusters.

D. Concept of Transition Radius

An analysis of Fig. 5(b) that represents the variation of the occupation probabilities as a function of the OASCS for both families at $r_s=0.08$ μm shows that there is no overlapping zone between the N_s and N_s+3 clusters, indicating that the σ_c remain small. Also, both DLCCA and RLPCA clusters lead to the same Gaussian fits, at least until $N_s=15$. Such behavior is also revealed upon inspection of Fig. 6(b) by remarking that the fractal dimension of the clusters seems to have a very small influence on the variation of $\langle C_{ext}\rangle_c$ as a function of N_s. Moreover, linear, RLPCA, and DLCCA clusters have an average OASCS that is very close to that under the isolated assumption. This confirms then the fact that this radius represents a transition where, for smaller and larger sizes, the $\langle C_{ext}\rangle_c$ is larger and smaller, respectively, than in the isolated case and that at this radius, each particle seems to scatter as if it were isolated from the others regardless of the fractal dimension. In other words, the electromagnetic coupling that comes from the interaction of the scattered fields is little affected by the cluster's configuration at this radius whereas it is strongly influenced for a larger or smaller one. We shall define the size of the constituent spheres at which such phenomena appear by the name transition radius.

Now, in Figs. 7(a) and 7(b), we present analogous results to those represented in Figs. 6(a) and 6(c) except that now the system under study is composed of latex particles in water. One can clearly observe that the influence of the fractal dimension discussed earlier on the variation of $\langle C_{ext}\rangle_c$ is still valid. However, for $r_s=0.132$ μm, all the aggregates still scatter more than the isolated particles even if the difference is smaller than that for $r_s=0.04$ μm. These results clearly indicate that the transition radius that we introduced earlier depends on the relative refractive index of the system (n_m/n_s), which is equal to 0.54 in the case of TiO_2 in a polymer resin and 0.89 for latex particles in water, and that for this latter system, the transition radius is superior to 0.132 μm.

To confirm this hypothesis, we performed a preliminary study, which consists in comparing the associated OASCS of two particles placed in contact with their isolated scattering cross section, varying r_s and the relative index of refraction, denoted N_{re}. The results of this study are shown in Fig. 8, where we plotted the transition radius, denoted R_t, as a function of N_{re}. The zone under the curve represents systems for which the OASCS is higher than that of isolated scatterers, whereas the zone above represents system parameters for which the OASCS is smaller than that of isolated scatterers. A curve passing through the points represents the transition between scattering

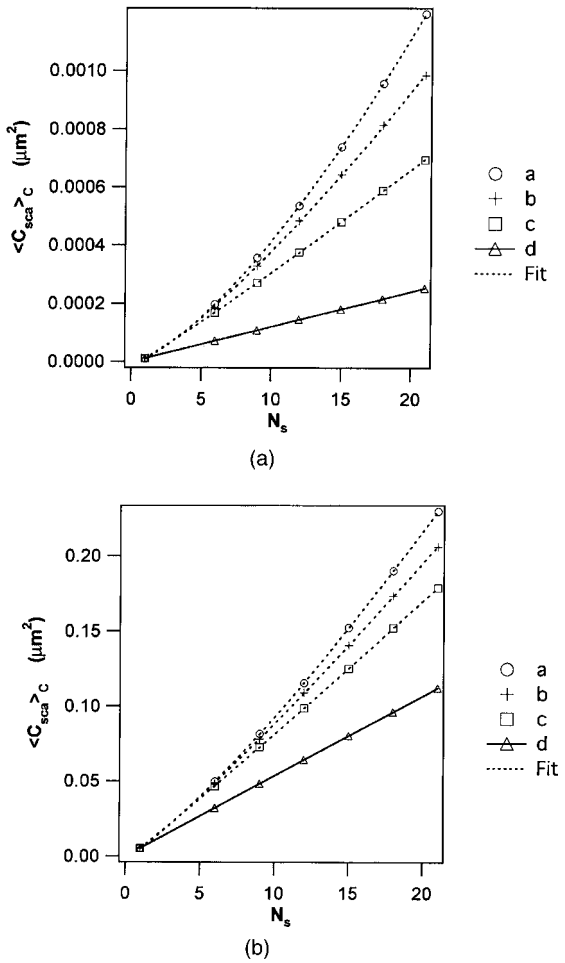

Fig. 7. (a) Variation of $\langle C_{ext}\rangle_c$ as a function of the number of particles for the (a) RLPCA, (b) DLCCA, and (c) linear chain with respective fractal dimensions of 3.0, 1.8, and 1.0, together with the value of $\langle C_{ext}\rangle_c$ in the case of isolated scatterers (d) for a cluster of latex particles in water. The radius of the constituent spheres is $r_s=0.04$ μm. (b) Same as (a) but for $r_s=0.132$ μm.

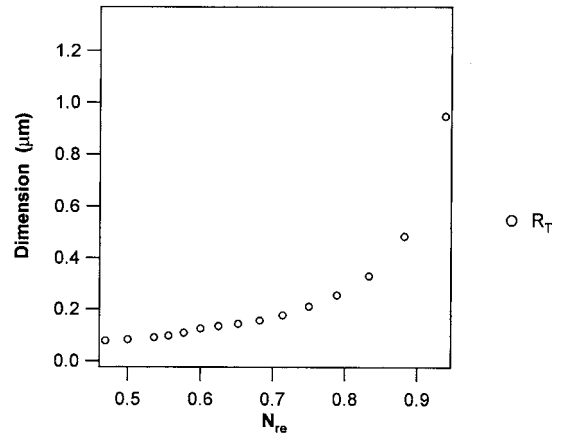

Fig. 8. Transition radius R_T as a function of relative refraction index N_{re} for a polymer resin host medium ($n_m=1.5$) and a wavelength of 0.546 μm.

regimes and thereby corresponds to the size regime for which where there is no apparent coupling between the spheres. The general tendency of this variation is that a more pronounced contrast of the index of refraction between the particles and the surrounding medium corresponds to a smaller transition radius. Thus one can see that the transition radius for latex particles in water occurs around 0.4 μm and that this is the reason that we could not observe it in the study illustrated in Fig. 7.

E. Extrapolation of the Orientation Average Scattering Cross Section for Larger Numbers of Constituent Spheres

Due to the large number of cluster configurations necessary to accurately evaluate the average optical parameters, the numerical calculations are quite time-consuming and studies on larger clusters cannot be considered. For this reason, the discussion in this subsection is devoted to the study of the extrapolated values of the OASCS for aggregates having much larger numbers of constituent spheres than in those that we studied previously. Results are shown for rutile titanium dioxide clusters in water with constituent spheres of $r_s=0.132$ μm.

Figure 9 represents the parameter $\langle C_{sca}\rangle_c$ normalized by the total volume of the aggregate, also denoted C^N_{sca}, as a function of the number of particles N_s for the linear, DLCCA, and RLPCA clusters. The use of this parameter is convenient because its variation as a function of the number of spheres in the cluster is a constant line parallel to the Ox axis for the isolated assumption. Two interesting tendencies can be observed. The first is that the variation of C^N_{sca} seems to converge to an asymptotic value, denoted $C^N_{sca,A}$, as N_s increases. The smaller the fractal dimension of the aggregate, the smaller the discrepancy compared with that in the isolated case and therefore the higher the value of $C^N_{sca,A}$. The second remark is that the number of particles N_s, denoted N_A, at which the variation of C^V_{sca} reaches its asymptotic value $C^V_{sca,A}$ increases with the fractal dimension of the aggregates. As we explained earlier, these observations reflect the strong correlation between the coupling effects and the average number of neighboring particles, and consequently with the fractal

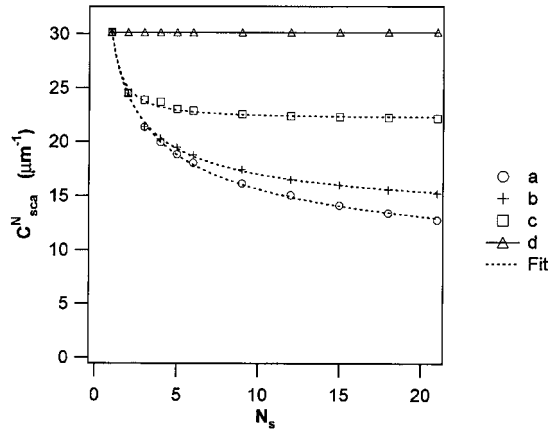

Fig. 9. Variation of C^N_{sca} as a function of the number of particles for the (a) RLPCA, (b) DLCCA, and (c) linear chain with respective fractal dimensions of 3.0, 1.8, and 1.0, together with the value of C^N_{sca} of isolated scatterers (d) for clusters of rutile titanium dioxide particles in water. The radius of the constituent spheres is $r_s=0.132$ μm.

Table 2. Adjustment Coefficients Given by the Power Law Functions

Coefficients	Linear	DLCCA	RLPCA
A_0	22.27	11.24	2.24
A_1	7.84	18.89	27.84
A_2	−1.75	−0.51	−0.31
χ	0.12	0.0035	0.043

dimension of the aggregate. The perturbation yielded by N_s+1 particles is weaker in a linear chain than in more compact configurations. For this reason, once that $\langle C_{sca}\rangle_c$ is normalized by the total volume of the cluster, the convergence is reached faster for a linear chain than for a compact configuration.

Taking into account those tendencies and variations, we have adjusted the data of Fig. 9 using a power law function such that $C_{sca}^N(N_s)=A_0+A_1N_s^{A_2}$. The values of coefficients A_0, A_1, and A_2 are shown in Table 2 for each adjustment. The asymptotic value and the convergence rate introduced earlier are given by the A_0 and A_2 coefficients, respectively. One can note that the quality of the adjustments is better for higher pseudofractal dimension; however, even for small dimensions, the root mean square error on the fit is still relatively small. For this reason, the extrapolation of the values C_{sca}^N could be performed with good precision for clusters composed of a number of primary particles N_s superior to 21 even if the asymptotic trend given by the power law is not exact and the variation of C_{sca}^N slowly increases with N.

5. CONCLUSION

The recursive centered T-matrix algorithm (RCTMA) was used to calculate the optical properties of nonspherical objects composed of aggregated spherical particles. We studied the orientation average scattering cross section (OASCS) of different types of clusters as functions of their size, refractive index contrast, pseudofractal dimension, and size of their constituent spheres. The variations of the optical properties were clearly linked to the different types and strengths of the electromagnetic couplings between the scattering objects. We have introduced the concept of transition radius, which defines the size of the constituent particles for which the overall cluster scattering of light behaves as the sum of the independent constituents. For larger and smaller sizes, the OASCS has stronger and lower values, respectively. Also, the transition radius depends very strongly on the relative refractive index of the scattering particles.

The OASCS that we have studied characterizes the strength of the scattering interaction with the cluster but does not give any information on the spatial distribution of the scattered energy. Such effects could be taken into account by evaluating the orientation scattering efficiency of the aggregates. This quantity is defined as the product of the scattering cross section by unit volume with the term $1-g$, where g represents the asymmetry parameters of the system.

Finally, further analysis should be carried out in order to retrieve C_{sca}^N as a function of the number of particles, using a simple function of the size of the constituent spheres, the relative index of refraction of the system, and the fractal dimension, without the obligation to perform a full statistical study based on RCTMA calculations.

APPENDIX A

The recursive algorithm of the RCTMA is given by

$$\bar{\bar{\tau}}_N^{(N,N)} = \left[\bar{\bar{\mathbf{I}}} - \bar{\bar{\mathbf{T}}}^{N(1)} \sum_{i=1}^{i=N-1} \bar{\bar{\mathbf{H}}}^{(N,i)} \sum_{j=1}^{j=N-1} \bar{\bar{\tau}}_{N-1}^{(i,j)} \bar{\bar{\mathbf{H}}}^{(j,N)}\right]^{-1} \bar{\bar{\mathbf{T}}}^{N(1)}, \tag{A1}$$

$$\bar{\bar{\tau}}_N^{(N,j)} = \bar{\bar{\tau}}_N^{(N,N)} \sum_{i=1}^{i=N-1} \bar{\bar{\mathbf{H}}}^{(N,i)} \bar{\bar{\tau}}_{N-1}^{(i,j)}, \quad j \neq N, \tag{A2}$$

$$\bar{\bar{\tau}}_N^{(k,i)} = \bar{\bar{\tau}}_{N-1}^{(k,i)} + \sum_{j=1}^{j=N-1} \bar{\bar{\tau}}_{N-1}^{(k,j)} \bar{\bar{\mathbf{H}}}^{(j,N)} \bar{\bar{\tau}}_N^{(N,i)}, \quad i \neq N, \tag{A3}$$

$$\bar{\bar{\tau}}_N^{(k,N)} = \sum_{j=1}^{j=N-1} \bar{\bar{\tau}}_{N-1}^{(k,j)} \bar{\bar{\mathbf{H}}}^{(j,N)} \bar{\bar{\tau}}_N^{(N,N)}, \quad i = N. \tag{A4}$$

ACKNOWLEDGMENTS

The authors thank Robert Botet for providing the source that was used to generate the cluster configurations, as well as Eduardo Nahmad and Adela Reyes for their support given to this work.

Jean-Claude Auger, the corresponding author, may be reached by e-mail at jcauger@cip.org.

REFERENCES

1. L. Tsang, J. Kong, and R. Shin, *Theory of Microwave Remote Sensing* (Wiley, 1985).
2. R. H. Zerull, B. A. S. Gustafson, K. Schultz, and E. Thiele-Corbach, "Scattering by aggregates with and without an absorbing mantle: microwave analog experiments," Appl. Opt. **32**, 4088–4100 (1993).
3. F. Borghese and P. Denti, "Electromagnetic scattering by a cluster of spheres," Appl. Opt. **18**, 116–120 (1979).
4. A.-K. Hamid, I. R. Ciric, and M. Hamid, "Iterative solution of the scattering by a system of multilayered dielectric spheres," IEEE Trans. Antennas Propag. **41**, 172–175 (1992).
5. A. Rahmani, C. Benoit, R. Jullien, G. Poussigue, and A. Sakout, "Light scattering in fractals with scalar and bond-bending models," J. Phys.: Condens. Matter **9**, 2149–2164 (1997).
6. M. Quinten and J. Stier, "Absorption of scattered light in colloidal systems of aggregated particles," Colloid Polym. Sci. **273**, 233–241 (1995).
7. S. Fitzwater and J. W. Hook III, "Dependent scattering theory: a new approach to predicting scattering in paints," J. Coat. Technol. **57**, 39–47 (1985).
8. Lord Rayleigh, "On the electromagnetic theory of light," Philos. Mag., 1881, pp. 12–81.
9. C. F. Bohren and D. R. Huffman, *Absorption and Scattering of Light by Small Particles* (Wiley-Interscience, 1983).
10. E. M. Purcell and C. R. Pennypacker, "Scattering and absorption of light by non-spherical dielectric grains," Astrophys. J. **186**, 705–714 (1973).

11. P. C. Waterman, "Matrix formulation of electromagnetic scattering," Proc. IEEE **53**, 805–812 (1965).
12. P. C. Waterman, "Symmetry, unitarity, and geometry in electromagnetic scattering," Phys. Rev. D **3**, 825–839 (1971).
13. M. A. Morgan and K. K. Mei, "Finite-element computation of scattering by inhomogeneous penetrable bodies of revolution," IEEE Trans. Antennas Propag. **AP-27**, 202–214 (1979).
14. P. P. Silvester and R. L. Ferrari, *Finite Elements for Electrical Engineers* (Cambridge U. Press, 1996).
15. K. S. Yee, "Numerical solution of initial boundary value problems involving Maxwell's equations in isotropic media," IEEE Trans. Antennas Propag. **AP-14**, 302–307 (1966).
16. A. Taflove, *Computational Electrodynamics: The Finite-Difference Time-Domain Method* (Artech House, 1995).
17. P. Yang and K.-N. Liou, "Finite-difference time domain method for light scattering by non spherical and inhomogeneous particles," in *Light Scattering by Nonspherical Particles: Theory, Measurements, and Applications*, M. I. Mishchenko, J. W. Hovenier, and L. D. Travis, eds. (Academic, 2000), pp. 173–221.
18. S. Chandrasekhar, *Radiative Transfer* (Dover, 1960).
19. U. Frisch, "Wave propagation in random media," in *Probabilistic Methods in Applied Mathematics*, A. T. Barucha-Reid, ed. (Academic, 1968), Vol. 1, pp. 75–191.
20. F. Curiel, W. Vargas, and R. G. Barrera, "Visible spectral dependence of the scattering and absorption coefficients of pigmented coatings from inversion of diffuse reflectance spectra," Appl. Opt. **41**, 5968–5978 (2002).
21. D. Bhanti, S. Manickavasagam, and M. P. Mengüç, "Identification of non-homogeneous spherical particles from their scattering matrix elements," J. Quant. Spectrosc. Radiat. Transf. **56**, 591–607 (1996).
22. M. I. Mishchenko, "Light scattering by size–shape distributions of randomly oriented axially symmetric particles of a size comparable to a wavelength," Appl. Opt. **32**, 4652–4666 (1993).
23. P. Rannou, C. P. McKay, R. Botet, and M. Cabane, "Semi-empirical model of absorption and scattering by isotropic fractal aggregates of sphere," Planet. Space Sci. **47**, 385–396 (1999).
24. R. Botet and P. Rannou, "Optical anisotropy of an ensemble of aligned fractal aggregates," J. Quant. Spectrosc. Radiat. Transf. **79-80**, 569–576 (2003).
25. R. Botet, P. Rannou, and M. Cabane, "Mean-field approximation of Mie scattering by fractal aggregates of identical spheres," Appl. Opt. **36**, 8791–8796 (1997).
26. J. C. Auger and B. Stout, "A recursive *T*-matrix algorithm to solve the multiple scattering equation: numerical validation," J. Quant. Spectrosc. Radiat. Transf. **79–80**, 533–547 (2003).
27. B. Stout, J. C. Auger, and J. Lafait, "A transfer matrix approach to local field calculations in multiple scattering problems," J. Mod. Opt. **49**, 2129–2152 (2002).
28. A. Ishimaru, *Wave Propagation and Scattering in Random Media* (Academic, 1978).
29. S. Stein, "Addition theorems for spherical wave functions," Q. Appl. Math. **19**, 15–24 (1961).
30. D. Mackowski, "Calculation of total cross sections of multiple-sphere clusters," J. Opt. Soc. Am. A **11**, 2851–2861 (1994).
31. B. Stout, J. C. Auger, and J. Lafait, "Individual and aggregate scattering matrices and cross-sections: conservation laws and reciprocity," J. Mod. Opt. **48**, 2105–2128 (2001).
32. J. C. Auger, R. G. Barrera, and B. Stout, "Scattering efficiencies of aggregates of spherical particles," J. Quant. Spectrosc. Radiat. Transf. **79–80**, 521–531 (2003).
33. R. Julien and R. Botet, *Aggregation and Fractal Aggregates* (World Scientific, 1987).
34. E. S. Thiele and R. H. French, "Light-scattering properties of representative, morphological rutile titania particles studied using a finite-element method," J. Am. Ceram. Soc. **81**, 469–479 (1998).